INTERNATIONAL JOURNAL FOR NUMERICAL METHODS IN FLUIDS
Int. J. Numer. Meth. Fluids **31**: 393–406 (1999)

THE USE OF OVERSET MESHES IN PARTICLE AND POROUS MEDIA THREE-DIMENSIONAL FLOWS

H.A. DWYER*, K. DeBUS AND N. SHAHCHERAGHI

Department of Mechanical and Aeronautical Engineering, University of California, Davis, CA 95616-5294, USA

SUMMARY

The overset grid technique has been illustrated with the use of several examples. These examples include droplet group dynamics, flow in porous media, and moving particles in pipes; the solutions have been accurate and efficient. The overset grid technique offers the advantages of high grid quality and a natural decomposition of multiple geometry problems onto parallel processors. For moving particles, the overset mesh technique seems to be particularly attractive since the need for remeshing is avoided. Copyright © 1999 John Wiley & Sons, Ltd.

KEY WORDS: overset meshes; three-dimensional flows; particle media; porous media

1. INTRODUCTION

The purpose of this paper is to simulate the steady and unsteady development of particle flows. These types of problems are important for energy systems using spray devices, such as diesel engines, as well as flows in porous media and for a wide range of solid particle applications in fluid dynamics. The numerical method used in the paper is based on the Chimera or overset grid technique, and it has proven to be efficient for these types of problems [1–4]. The present calculations have used up to 300 particles and they have been carried out on a wide variety of both serial and parallel computers. However, it is not possible to do a complete numerical simulation of spray systems or porous media in the immediate future owing to the excessive complexities that occur in practical systems. What can be accomplished is the beginning of a physical understanding of group interactions in particle systems, and if this understanding is used correctly the knowledge can be applied to some parts of a practical spray. It is the authors' belief that the main challenge of the future will be to design numerical simulations that are reduced in scale, but yet contain the essence of the physical processes of particle behavior.

The present results include three different fluid flows, and in the most complicated case variable gas and liquid properties were employed, as well as finite rate chemical kinetics. We have restricted these first studies to intermediate and small Reynolds numbers, since this regime has, and will have, a key role in particle dynamics. The use of overset meshes has led to a significant simplification of the mesh generation needed for groups of particles, and it allows the use of efficient equation solvers for structured meshes. Also, the grid quality can be

* Correspondence to: Department of Mechanical and Aeronautical Engineering, University of California, Davis, CA 95616-5294, USA.

CCC 0271–2091/99/170393–16$17.50

excellent since the majority of overset grids employed have been body-fitted and are orthogonal near solid surfaces. Another feature of the overset grid technique is that it automatically defines a domain decomposition scheme, and this feature has been used on parallel processors to obtain solutions.

2. METHOD OF APPROACH AND EQUATIONS

The starting point for the investigation is the low Mach number form of the Navier–Stokes equations in control volume form. The purpose of the low Mach approximation is to eliminate acoustic waves and time scales from the problem, and this allows the numerical integration to proceed at the slower time scale of the diffusion and convection processes [5]. For three-dimensional flow with a time-dependent and accelerating mesh, the equations can be written in the control volume integral form

$$\frac{\mathrm{d}}{\mathrm{d}t}\iiint_V \rho\,\mathrm{d}V + \iint_A \rho(\vec{V}-\vec{V}_b)\cdot\mathrm{d}\vec{A} = 0,$$

$$\iiint_V \rho\frac{\partial u}{\partial \tau}\,\mathrm{d}V + \iiint_V \rho(\vec{V}-\vec{V}_b)\cdot\vec{\nabla}u\,\mathrm{d}V = \iint_A p\hat{i}\cdot\mathrm{d}\vec{A} + \iint_A \bar{\bar{\tau}}\cdot\hat{i}\,\mathrm{d}\vec{A},$$

$$\iiint_V \rho\frac{\partial v}{\partial \tau}\,\mathrm{d}V + \iiint_V \rho(\vec{V}-\vec{V}_b)\cdot\vec{\nabla}v\,\mathrm{d}V = \iint_A p\hat{j}\cdot\mathrm{d}\vec{A} + \iint_A \bar{\bar{\tau}}\cdot\hat{j}\,\mathrm{d}\vec{A},$$

$$\iiint_V \rho\frac{\partial w}{\partial \tau}\,\mathrm{d}V + \iiint_V \rho(\vec{V}-\vec{V}_b)\cdot\vec{\nabla}w\,\mathrm{d}V = \iint_A p\hat{k}\cdot\mathrm{d}\vec{A} + \iint_A \bar{\bar{\tau}}\cdot\hat{k}\,\mathrm{d}\vec{A},$$

$$\iiint_V \rho C_p\frac{\partial T}{\partial \tau}\,\mathrm{d}V + \iiint_V \rho C_p(\vec{V}-\vec{V}_b)\cdot\vec{\nabla}T\,\mathrm{d}V$$
$$= \iint_A k\vec{\nabla}T\cdot\mathrm{d}\vec{A} - \iiint_V \rho\sum_{i=1}^{kk} Y_i C_{p,i}\vec{V}_i\cdot\vec{\nabla}T\,\mathrm{d}V - \iiint_V \sum_{i=1}^{kk} h_i\dot{\omega}_i W_i\,\mathrm{d}V,$$

$$\iiint_V \rho\frac{\partial Y_i}{\partial \tau}\,\mathrm{d}V + \iiint_V \rho(\vec{V}-\vec{V}_b)\cdot\vec{\nabla}Y_i\,\mathrm{d}V = \iint_A \rho Y_i\vec{V}_i\cdot\mathrm{d}\vec{A} + \iiint_V \dot{\omega}_i W_i\,\mathrm{d}V,$$

where notations are given in Appendix A.

The gas phase was assumed to obey the ideal gas law and the thermodynamic and transport properties were obtained from the CHEMKIN subroutines [6]. The liquid properties were obtained from [7]; however, the liquid species mass diffusion coefficients were obtained from an assumed Lewis number and a calculated thermal diffusivity. The details of the present formulation can be found in papers by Niazmand *et al.* [8] and Dwyer [9]. The numerical methods employed for the solution of the system of equations are second-order accurate in time and space, and they make use of a predictor–corrector scheme developed by Dwyer [5].

3. RESULTS

The paper will show three examples of the particle and droplet calculations we have performed. These flows are (1) unsteady heating and vaporization of a droplet group; (2) steady flow in a pipe filled with a group of spherical particles; and (3) the unsteady heating of a spherical particle moving in a pipe flow. Each one of these flows exhibits a favorable feature of the overset grid technique. We will now present the three examples.

3.1. Unsteady heating and vaporization of a droplet group

The first example is concerned with a group of six heptane droplets that are arranged in a plane as shown in Figure 1 [9,10]. This figure shows the mesh's plane of symmetry, i.e. the plane, and there are 13 separate three-dimensional meshes. The specific meshes are the large major mesh, the six internal droplet meshes and the six surrounding droplet meshes. The meshes surrounding the droplets couple the flow to the outer main mesh, and interpolation is used to connect the flow variables between the inner and outer meshes. These fine meshes around each droplet capture the flow near the high gradient droplet surface, and they can be considered as a viscous layer mesh. Since the calculations include mass transfer, the size of the droplets changes in time, and a grid velocity term, $\vec{V}_b$, was added to the equations of motion for all variables. For applications involving modern diesel engines, the assumption of a spherical shape is a good one due to the small droplet size and relatively large surface tension forces.

The droplets have an initial diameter of 50 μm, and they are injected into a hot air flow (1000 K; 20 atmospheres). We begin the discussion early on in the simulation, and the droplets have lost approximately 3% of their mass. The temperature and fuel mass fraction contours in the plane of symmetry of the flow are given in Figures 2 and 3 respectively. The temperature contours in Figure 2 show a region of cooled fluid around the droplet group which has been extended a short region downstream by convection. The heptane fuel mass fractions contours in Figure 3 have been limited to a maximum value of 0.25 in order that the pure fuel values of the liquid do not dominate the presentation. At this time in the simulation, chemical reactions in the group wake have increased the temperature above the incoming free stream temperature of 1000 K, and the maximum temperature in the group wake is 1017 K. In general, there is significant a penetration of fluid into the droplet group, and this can be seen in both Figures 2 and 3. However, a deeper understanding of the fluid dynamics of the group interaction can be obtained by studying the three-dimensional dynamic pressure field contours on the droplet surfaces shown in Figure 4. The two front droplets have large pressures at the front stagnation points; however, the rear droplet pressure distributions have been influenced by the front droplets. This influence has decreased the stagnation pressure, since the velocity inside the group is less than the free stream velocity.

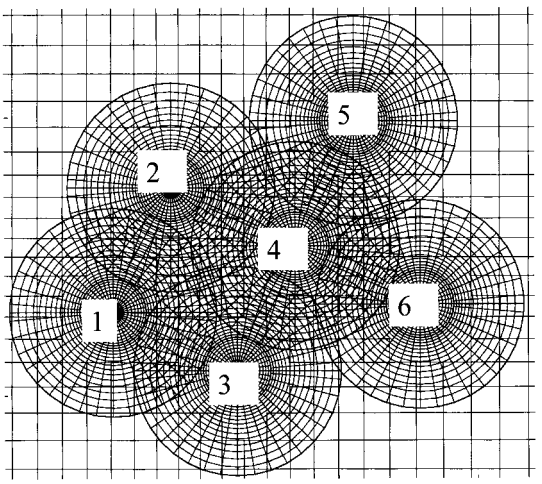

Figure 1. Mesh for heptane droplet group at $Re = 5$; $P = 20$ bar; $T = 1000$ K; $D = 50$ μm; time = 0.294 ms. Symmetry plane results.

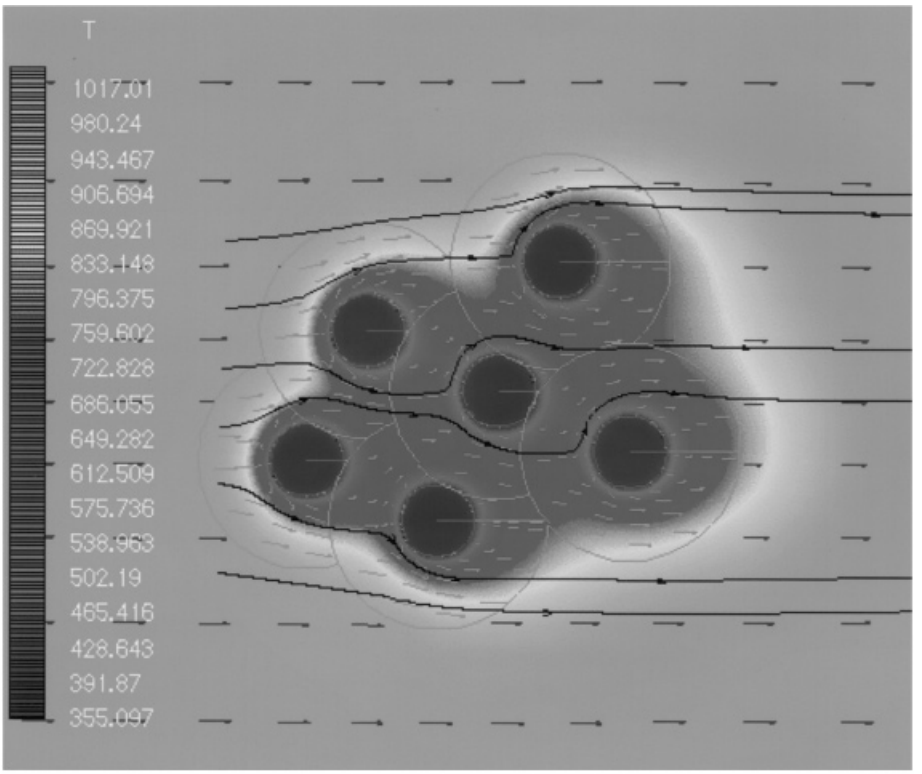

Figure 2. Temperature contours for heptane droplet group at $Re = 5$; $P = 20$ bar; $T = 1000$ K; $D = 50$ μm; time = 0.294 ms. Symmetry plane results.

Further along in the simulation, approximately three times longer, there is a significant fuel burning in the droplet wake, and the wake maximum temperature has risen to a value close to 2200 K (Plate 1). Plate 1 shows the solution at three different mesh densities, and it is clear that the solution is converged in both space and time. It can be seen from these numerical experiments that the trilinear interpolation used with the overset grid technique is accurate in space, and it has not led to time-dependent phase errors in the solution. At the physical time shown in Plate 1, the maximum and minimum mass loses for the droplets were 13% and 7%, and the maximum gas phase fuel mass fractions have reached values of almost 0.50. It can be clearly seen in Plate 1 that the reacting flow region has moved very close to the droplet group, and on the bottom side of the rear droplet, it is moved into the droplet mesh. The temperature contours in Plate 1 are dominated by the reaction zone in the wake, however, all temperatures inside the droplet group are low. The shape of the reacting zone is influenced by the distribution of fuel in the droplet wake, and the combustion process moves around the edges of the group, however, the fuel richness of the wake directly behind the group delays the forward flame propagation.

Some very important quantities for spray modeling are the droplet global coefficients, such as drag, Nusselt number and droplet mass history for the individual droplets in a group. The time history of the droplets drag coefficient is shown in Figure 5, and the identifying numbers associated with the individual droplets are given in Figure 1. The influence of the group behavior is to cause a difference in the drag coefficient of a factor of two between the droplets.

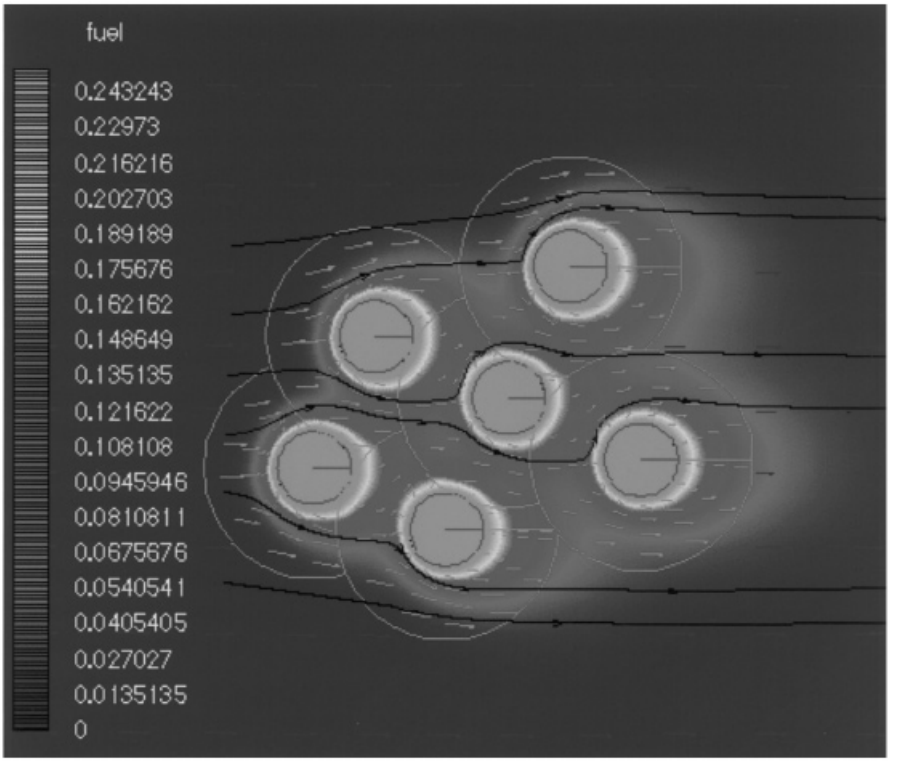

Figure 3. Fuel contours for heptane droplet group at $Re = 5$; $P = 20$ bar; $T = 1000$ K; $D = 50$ μm; time = 0.294 ms; maximum mass fraction = 0.25. Symmetry plane results.

The influence of the reaction zone can be seen on droplet number 6, and the increase in the drag coefficient should be noted.

3.2. Porous media flow

The next example presented is the flow in a pipe filled with spherical particles [11,12]. A simulation with a small number of particles is given for visual purposes in Figure 6, where 20 spheres are randomly placed in a pipe at a Reynolds number of 1. Twenty was a reasonable number of particles to use on a single processor, however, this number changes with the advances made in the single processor speed. The fluid is incompressible and the properties are constant for the porous media simulations. A major complication of this flow geometry is that the particles touch or nearly touch both themselves and the pipe wall, and this causes a potential grid generation problem. In this study, we have chosen the outer part of the particle mesh to fit to the neighboring particle or wall. This has the advantage that the outer mesh fringe points have the no-slip boundary condition, and it avoids the need to interpolate values to these boundary points. The isobars of pressure in Figure 7 show a progression from high to low values, and the velocity vectors are quite complex due to the interactions between particles and walls. It should be mentioned that porous media calculations of this type must be started from a zero velocity condition, and the overall pressure drop specified. Any attempt to start the calculation from a given mass flow yields excessive pressure gradients and extremely slow convergence of the Poisson equation. It should be obvious that any assumption

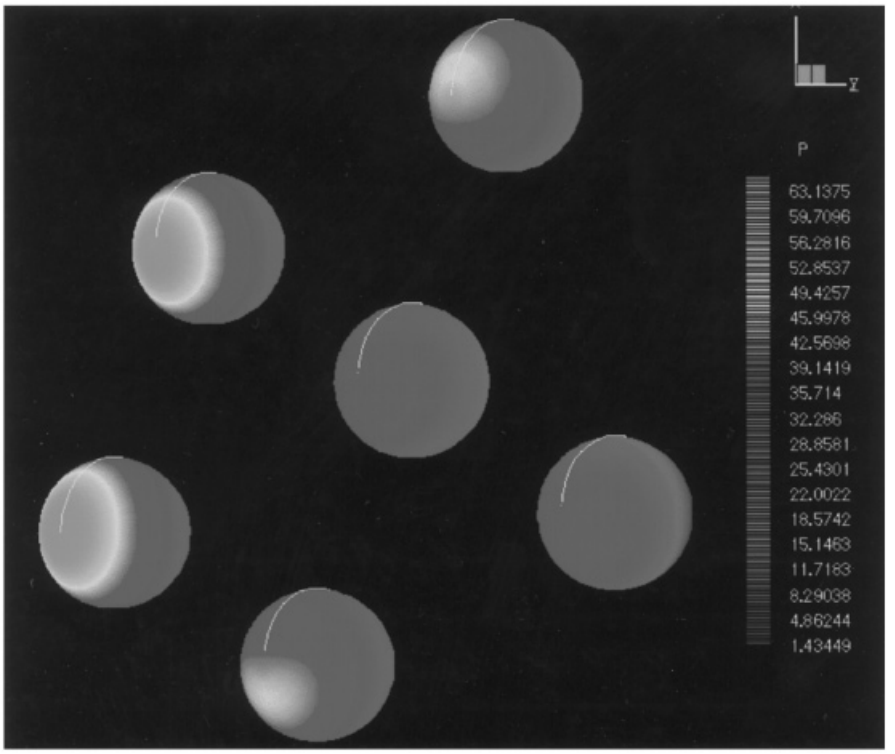

Figure 4. Surface pressure contours for heptane droplet group at $Re = 5$; $P = 20$ bar; $T = 1000$ K; $D = 50$ μm; time = 0.902 ms.

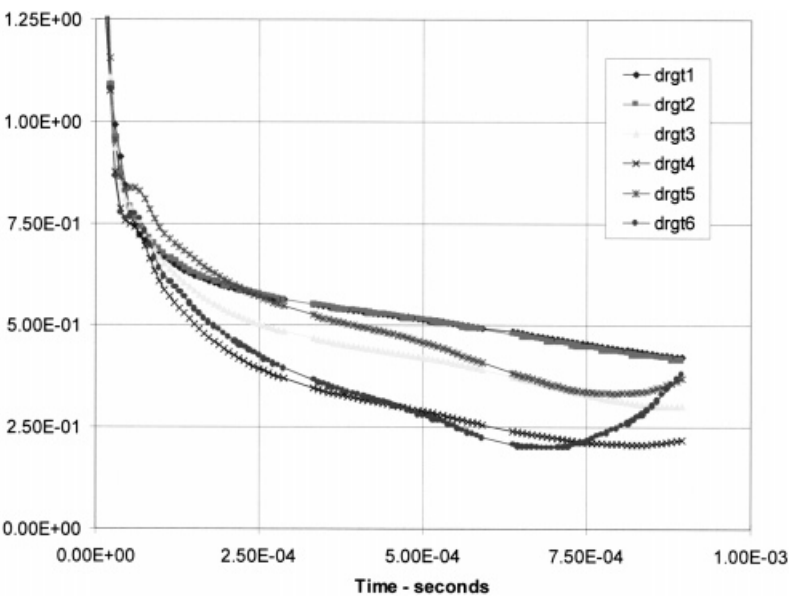

Figure 5. Variation of normalized total drag as a function of time, $Re = 5$, $P = 20$ bar. The results are normalized with a steady incompressible flow at $Re = 5$.

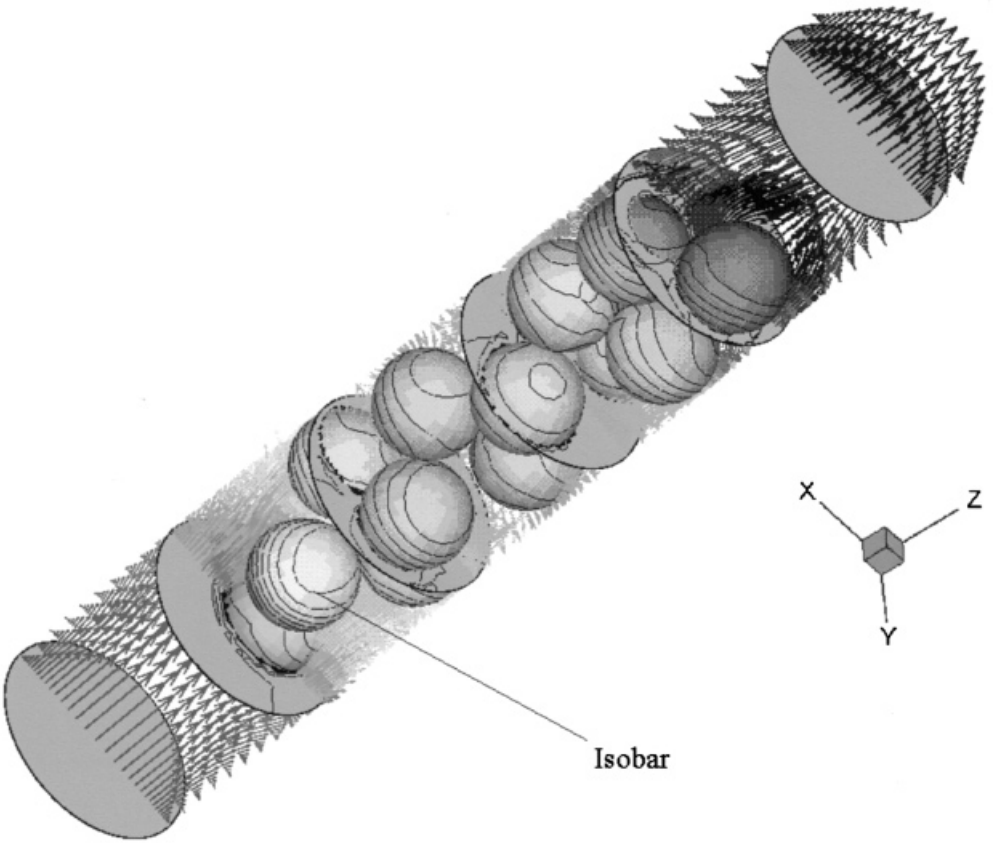

Figure 6. Simulation of 20 spheres in a pipe, $Re = 1$; $D/d_p = 1.4$. Pressure isobars and velocity vectors.

for the initial velocity distribution in the porous media will lead to very large initial errors in the Navier–Stokes equations.

The specific mesh scheme that was utilized for the porous media calculations was quite unique for overset grid methods, and it will now be briefly described. In most overset grid simulations, the individual meshes are generated independent of each other, as shown in Figure 1. However, for a simulation of a porous media flow, the particle density is very high and the generation of independent meshes leads to many invalid points inside solid objects and very poor resolution near the sphere touching locations. The actual meshing scheme used consisted of a two-step process that first generated independent spherical meshes and then corrected these meshes for better resolution and to remove the invalid points. The mesh correction algorithm consisted of using a bisection algorithm to move the invalid points from outside the pipe wall or inside a particle to the wall or particle surface. At locations near the touching of the particles all the mesh points radial to a sphere surface are placed between two spheres, and the mesh resolution becomes very fine. Of course, at or near a point of touching, the mesh becomes singular and physical approximations must be employed. For example, we choose to let the spheres touch in order to a get lower porosity, and we constrained all mesh locations within a small angle of the touching location to have a no-slip or zero velocity condition. In general, we have had excellent results with this procedure, and we have not had to use numerical dissipation schemes in any of the porous media simulations.

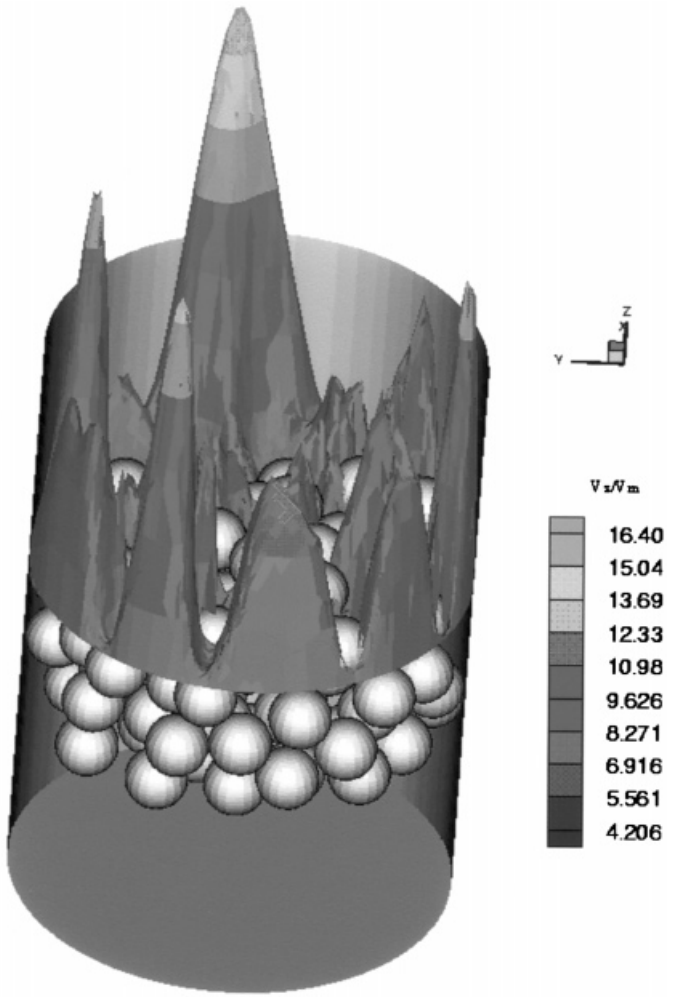

Figure 7. Simulation of 120 spheres in a pipe. $Re = 23$; $D/d_p = 7$. Axial velocity profile.

If the number of particles is increased to 120 and the diameter of the pipe is also increased, we obtain a simulation that is interesting to workers in the field of porous media flow, see Figure 7 and Plate 2. In Figure 7, we show the magnitude of the axial velocity near the exit plane of the porous media for a pipe Reynolds number of 23 based on the average flow velocity. It is immediately evident that the velocity field varies significantly from normal pipe flow or Darcy's law, since the maximum velocity reaches a value greater than 16 times the mean velocity. These maximum velocities tend to occur near the pipe wall, and this can be shown to be a result of the random packing of the spheres near the wall. Decreasing the size of the spheres relative to the pipe diameter will cause this effect to be less pronounced. The pressure distributions in Plate 2 show a more regular variation compared with the smaller number of spheres in Figure 6. It should also be noted that there are sharper gradients near the inlet and exit of the porous media. A detailed surface plot of the exit plane axial velocity is given in Figure 8, and it is seen that the magnitude of the velocity is variable over the entire cross-section of the pipe.

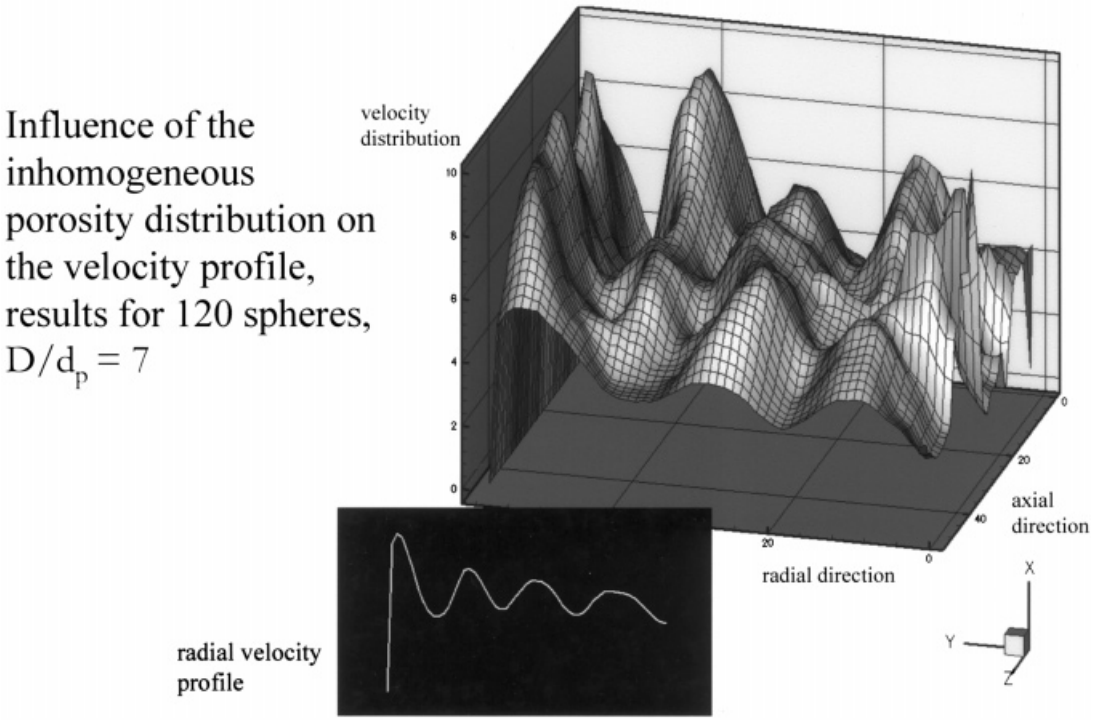

Figure 8. Axial velocity distribution in porous media. $Re = 23$.

If the number of particles is increased to 300 and the Reynolds number varied over a significant range, the average pressure drop in the pipe can be compared with semi-empirical equations [13] as shown in Figure 9. In general, the numerical simulations give good results, however, they are somewhat high in their values. Considering the limited number of particles, and the problems of numerically packing the pipe, the results are excellent. The simulation also has the ability to carry out sensitivity studies and to extend the work to heat and mass transfer.

The last topic to be discussed is the use of parallel processing to accomplish the calculations presented in this paper. Shown in Figure 10 are the results of using three DEC Alpha Workstations using a PVM system [14], and it should be noted that the computer code was written in Fortran. Also shown in Figure 10 is the relative time per iteration of the entire mesh as a function of the number of spherical particles. Since the individual spheres consist of overset meshes with the same number of grid points it was not difficult to distribute the load between processors. After the number of particles has increased to a number greater than 12, the PVM-driven system achieves results approximating the one-half and one-third the theoretical values of speed-up. The primary reason for not approaching theoretical values was the main mesh, which was not parallelized in the simulations. For the simulations employing 120 and 300 spherical particles, the code was ported to a six processor DEC Alpha system and a 16 processor Cray T3E. The parallel performance on these platforms was similar to the results shown in Figure 10.

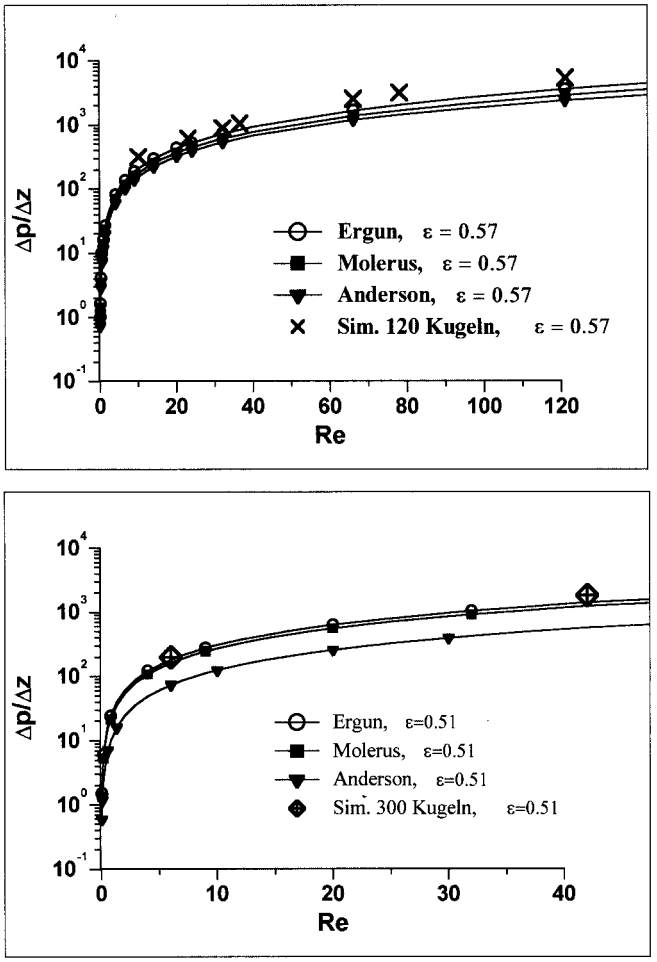

Figure 9. Average axial pressure in porous media. Comparison with empirical correlations for various Reynolds numbers and porosities.

3.3. Heat transfer to moving particles in pipe flow

Another flow problem where the overset approach is quite attractive is that of moving meshes, and an interesting problem is the heating of a particle moving in a pipe. A fully developed pipe flow subjected to wall heating is shown in Figure 11. The wall heating begins a thermal boundary layer, and the thermal boundary layer heats a rotating spherical particle that is moving at constant velocity in the pipe. The sphere is moving at the local mean pipe velocity at its centroid, and the rotation rate is equal to that of the fluid. The fluid flow over the sphere is steady; however, the heat transfer problem is unsteady. Without the use of an overset mesh, this problem would be quite complex due to the need to remesh as the particle moves in the pipe.

The initial conditions for the flow problem are the steady solution of the rotating sphere–wall interaction and the thermal entrance problem in the pipe. The spherical particle with its overset mesh is then introduced upstream of the thermal boundary layer region, and the overset spherical mesh is passed through the pipe thermal boundary layer mesh. The

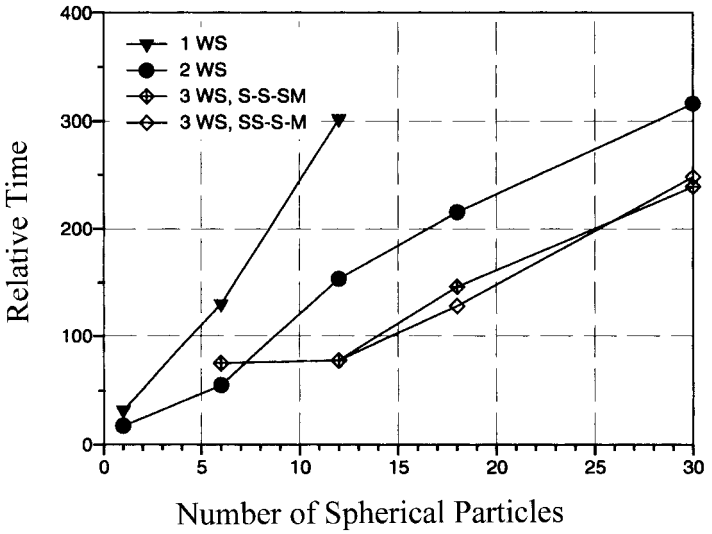

Figure 10. Parallelization study on DEC workstations.

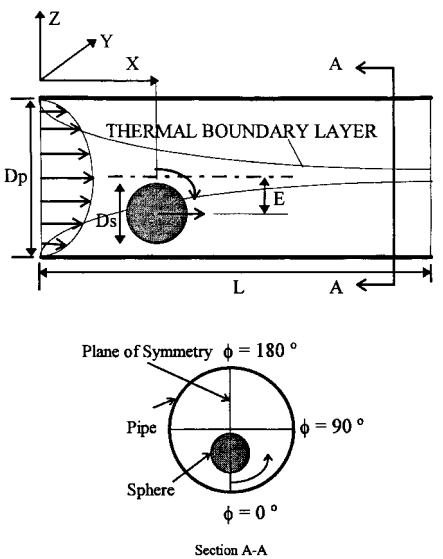

Figure 11. Geometry of moving sphere in heated pipe.

solution procedure consists of solving the unsteady thermal energy equation between the pipe and spherical overset mesh. A typical solution is shown in Plate 3, where the temperature isotherms are presented at various locations down the pipe. The results in Plate 3 are for a relatively large particle, and a pipe Peclet number of 100 based on the average velocity of the pipe flow. The largest amount of heating occurs near the start of the thermal entrance region, and decreases as the sphere increases in temperature. The average Nusslet number for the spherical particle is given in Figure 12 for various Peclet numbers and size particles. In general, the larger particles and Peclet numbers cause increased heating, however, the smaller particles have unusual behavior as they interact with the thermal boundary layer of the pipe [14,15].

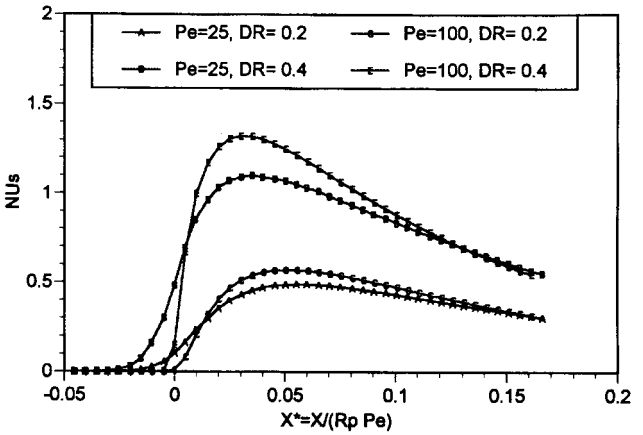

Figure 12. Average sphere Nusselt number along the pipe as a function of Peclet number and diameter ratio.

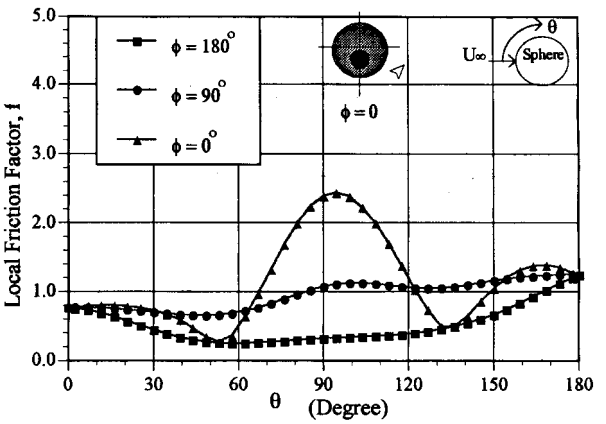

Figure 13. Sphere local friction factor as a function of angular position. $Pe = 100$; $d_p/D = 0.4$.

In this paper we do not have time to present more detailed results, however, the entire structure of the flow and heat transfer has been determined for the sphere and pipe surfaces. An example of this structure is given in Figure 13, where the local skin friction on the sphere surface is given at three angular positions. A very interesting behavior is shown where the sphere is near the pipe wall. At this location the flow initially slows due to blockage, then it speeds up due to a minimum area. This is followed by the flow slowing down, which is caused by an area expansion. The real advantage of the overset approach is the good mesh quality obtained from the simple spherical and pipe meshes. Also, the structured nature of the meshes allows for efficient solvers and a logical decomposition for use on parallel computers.

4. FUTURE POSSIBILITIES

The present authors have good hopes for simulating much larger groups of particles and droplets with the use of parallel processor computing techniques. The present calculations were carried out on simple serial and parallel machine systems, and the effort needed to port the

code to a parallel machine was minimal. The use of the overset grid technique allows for a natural domain decomposition of the particles and droplets into individual processors, and the possibility of tens of thousand of droplets is quite feasible. With the development of faster processors in the near future, the possibilities seem very good. However, even with this computer power, the numerical simulations will have to be designed very carefully to get useful statistical information. It is the authors' opinion that only sections and important edge regions will be able to be systematically studied, and that this information will have to be carefully transferred to particle and spray technology.

5. CONCLUSIONS

The important conclusions of the research are

(1) The overset or Chimera grid technique has shown itself to be an efficient technique for treating the very complicated problems of particle and droplet group interactions. The natural decomposition of the particle and droplets into small spherical grids allows for the treatment of large numbers, since it lends itself to future parallel processing in an efficient manner.

(2) The complex problem of group interaction between heating and vaporizing droplets has been studied in detail. For this problem variable properties and chemical reactions where included in the overset grid simulation.

(3) The problem of flow in porous media has been treated with the use of overset grid techniques. Flow simulations with 300 particles exhibit the behavior of porous flows over an important Reynolds number regime.

(4) Moving mesh problems offer excellent opportunities for overset grid techniques. The thermal heating of a spherical particle in a pipe has been treated in an accurate and efficient way.

APPENDIX A. NOMENCLATURE

$\vec{A}$	area
A_{p}	droplet projected area
A_{s}	droplet surface area
C_{D}	drag coefficient
C_p	specific heat
D	droplet diameter
h_i	enthalpy of species i
k	thermal conductivity
Nu	global Nusselt number
Nu_i	local Nusselt number
p	flow dynamic pressure
Re	Reynolds number ($=\rho_\infty U_\infty D/\mu_\infty$)
$\vec{s}$	surface tangent vector
t	time
T	temperature
T_{s}	droplet surface temperature
u	x velocity component
v	y velocity component
$\vec{V}$	fluid velocity vector

$\mathrm{d}V$	volume
$\vec{V}_b$	mesh velocity vector
$\vec{V}_i$	diffusion velocity of species i
w	z velocity component
W_i	molecular weight of species i
$Y_i = (m_i/m_T)$	mass fraction of species i
ρ	density
$\bar{\bar{\tau}}$	stress tensor
$\dot{\omega}_i$	molar production rate of species i

REFERENCES

1. J.A. Benek, J.L. Steger, F.C. Dougherty and P.G. Buning, 'Chimera, a grid embedding technique', *AEDC-TR-85-64*, Arnold Air Force Station, TN, 1986.
2. F.C. Dougherty, 'Development of a grid scheme with applications to unsteady problems', *Ph.D. Thesis*, Stanford University, 1985.
3. P.G. Buning, I.T. Chiu, S. Obayashi, Y.M. Rizk and J.L. Steger, *AIAA Atmospheric Flight Mechanics Conference*, Minneapolis, MN, *AIAA Paper-88-4359-CP*, 1988.
4. H. Nirschl, H.A. Dwyer and V. Denk, 'Three-dimensional calculations of the simple shear flow around a single particle between two moving walls', *J. Fluid Mech.*, 273–285 (1995).
5. H.A. Dwyer, 'Calculations of droplet dynamics in high temperature environments', *Prog. Energy Combust. Sci.*, **15**, 131 (1989).
6. R.J. Kee, F.M. Rupley and J.A. Miller, CHEMKIN II, *Report SAND 89-8009*, Sandia National Laboratory 1990; and R.J. Kee, F.M. Rupley, G. Dixon Lewis, J. Warnatz, M.E. Coltrin and J.A. Miller, *Report SAND 86-8246*, Sandia National Laboratories, 1986.
7. R.C. Reid, J.M. Prausnitz and B.E. Poling, *The Properties of Gases and Liquids*, Fourth edn., McGraw-Hill, New York, 1987.
8. H. Niazmand, I. Aharon, B.D. Shaw and H. Niazmand, 'Surface tension influences on methanol droplet vaporization in the presence of water', *26th Int. Symp. on Combustion*, Naples, Italy, 1994, pp. 1613–1619.
9. H.A. Dwyer, H. Nirschl, P. Kerschl and V. Denk, 'Heat, mass, and momentum transfer about arbitrary groups of particles', *25th Int. Symp. on Combustion*, The Combustion Institute, 1994.
10. H.A. Dwyer and P. Stapf, 'Unsteady vaporization and ignition of a three-dimensional droplet array', *Proc. 3rd Workshop on Modeling of Chemical Reaction Systems*, Heidelberg, Germany, 24–26 July 1996; also submitted to *Combustion and Flame*.
11. K. Debus, *Ph.D. Thesis*, Lehrstuhl fur Fluidmechanik und Prozeßautomation, Technische Universität München, December 1997.
12. K. Debus, H. Nirschl, A. Delgado and V. Denk, 'Three-dimensional calculations of flow through packed beds', *7th Inter. Sym. on CFD*, Peking, China, September 1997.
13. S. Ergun, 'Fluid flow through packed columns', *Chem. Eng. Prog.*, **48**, 89–94 (1952).
14. N. Shahcheraghi, 'Numerical study of three-dimensional incompressible flow and heat transfer over a stationary and moving sphere in a pipe', *Ph.D. Thesis*, University of California at Davis, June 1996.
15. N. Shahcheraghi and H.A. Dwyer, 'Fluid flow and heat transfer over a spherical object in a pipe', *ASME J. Heat Transf.*, **120**, 985 (1998).

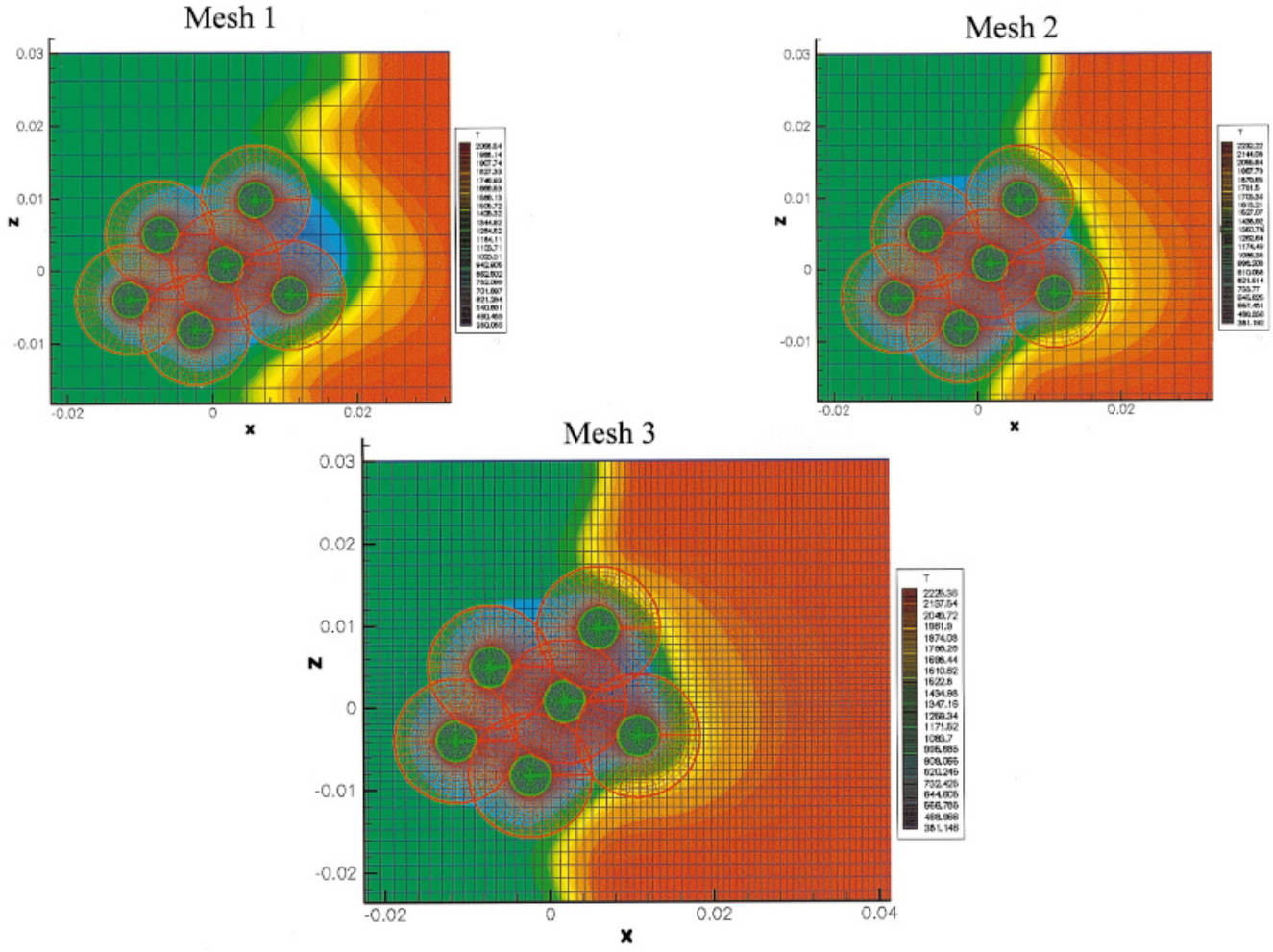

Plate 1. Mesh resolution study of chemical reactions.

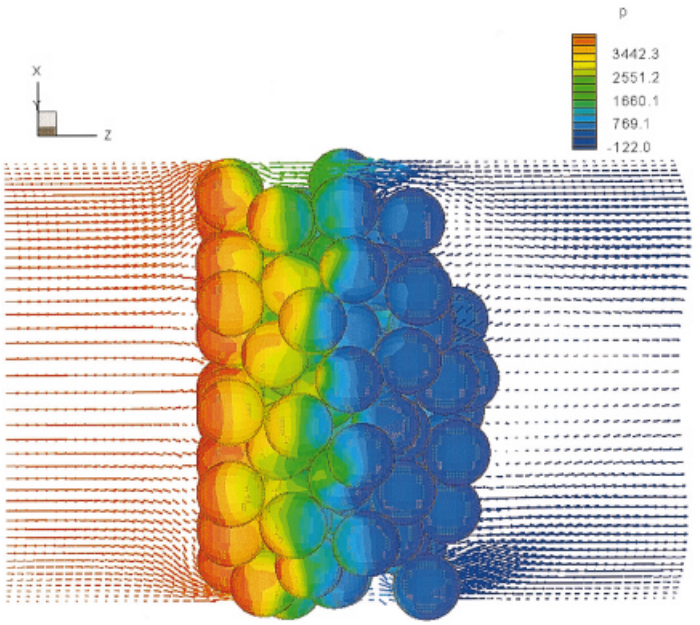

Plate 2. Isobars for 120 spheres in a pipe. $Re = 23$; $D/d_p = 7$.

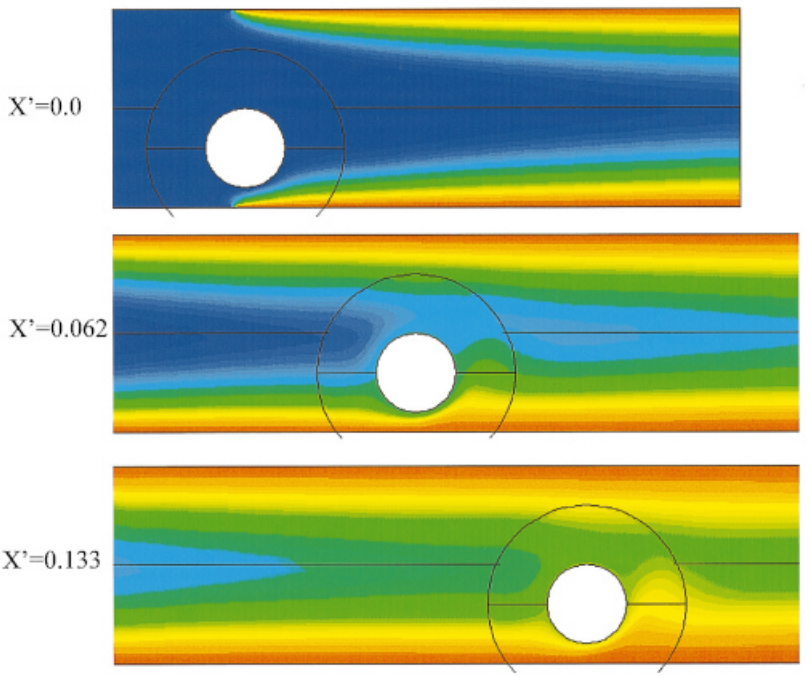

Plate 3. Temperature isotherms vs. distance along the pipe. $Pe = 100$; $d_p/D = 0.4$.